Study of Au coated ZnO nanoarrays for surface enhanced Raman scattering chemical sensing

Grégory Barbillon, Vinod E Sandana, Christophe Humbert, Benoit Belier, David J Rogers, Ferechteh H Teherani, Philippe Bove, Ryan Mcclintock, Manijeh Razeghi

Journal Name

ARTICLE TYPE

Cite this: DOI: 10.1039/xxxxxxxxxx

Study of Au coated ZnO Nanoarrays for Surface Enhanced Raman Scattering Chemical Sensing.

Grégory Barbillon,*[a] Vinod E. Sandana,[b] Christophe Humbert,[c] Benoit Bélier,[b] David J. Rogers,[b] Ferechteh H. Teherani,[b] Philippe Bove,[b] Ryan McClintock[d] and Manijeh Razeghi [d]

Received Date
Accepted Date

DOI: 10.1039/xxxxxxxxxx

www.rsc.org/journalname

Eight 1 cm^2 samples of self-organising ZnO nanopillar arrays with preferential vertical orientation were grown by pulsed laser deposition and then coated with 30 nm of Au using either thermal or electron-beam evaporation. Each sample had a different set of ZnO and Au growth conditions. The Au/ZnO nanoarrays were then tested for use in surface enhanced Raman scattering (SERS) detection of thiophenol molecules. The ratio of I_{SERS}/I_{Raman} was adopted as a measure of the SERS sensitivity and was found to vary from 1.7 to 23.7 within the 8 samples. The impact of the density, width, filling factor, orientation, homogeneity and shape of the nanostructures on the average SERS intensity and the within-wafer reproducibility of the SERS response were considered for 9 paired comparisons based on fixing all but one of the growth parameters for each pairing. Overall, smaller nanopillar width was found to correlate with stronger average SERS signal while more vertically aligned arrays with higher filling factors showed better within-wafer reproducibility.

1 Introduction

At present, the simultaneous attainment of good reproducibility and high enhancement factors (EF) are key challenges in the development of surface enhanced Raman scattering (SERS) substrates for improved chemical and biological sensing. SERS substrates are generally based on distributions of metallic nanoparticles/structures with different shapes and architectures which are prepared by either thermal dewetting, precipitation from colloidal suspensions [1–4] or advanced (e.g. deep UV or electron beam (EBL)) lithographic techniques [5–9]. Although such substrates can exhibit large Raman enhancements, the former two techniques (colloidal and thermal dewetting) give poor SERS reproducibility while deep UV and EBL are too expensive and/or complex for mass production [10–14]. Other (potentially lower cost) approaches such as Nanoimprint Lithography (NIL) [15–17] and NanoSphere Lithography (NSL) [18–20] can be employed to fabricate these SERS substrates but they are plagued by poor nanostructure definition on the relatively large scale of the surfaces that are required for practical SERS substrates applications. Recently, arrays of nanowires decorated with metallic nanoparticles have been proposed as SERS substrates with an improved detection limit [21–24]. For example, silicon nanoarrays coated with silver nanoparticles were studied by Galopin *et al* [25]. In this case, regular arrays of Si nanowires were realized through a high-temperature vapor–liquid–solid (VLS) growth. Although a high SERS response was observed, such a VLS approach is relatively expensive and Ag nanoparticles are readily oxidised in air, so the functional lifetime of such substrates is rather limited. In this paper, SERS substrates are formed by coating nanostructured ZnO templates with a layer of gold and the performance is correlated with the nanoarray scale, morphology, homogeneity, filling factor and orientation. ZnO was selected for the study because of a propensity for nanostructuration combined with a relatively high refractive index ($\sim$ 2 in the visible spectrum), which confines the light and thus enhances the SERS effect. Capping layers of gold provided the plasmonic activity to the ZnO nanostructures. Gold was selected because of a combination of a suitable plasmonic resonance, a favourable surface chemistry and a resistance to oxidation. Gold also allows functionalizations which are suitable for various applications, including medical diagnosis and bioassays. Although several groups have already worked on hybrid (metal/ZnO) nanostructures for SERS sensing [26–30], there was little consideration of the effects of the nanostructure scale, orientation and morphology on the SERS performance. In this paper, the effects of the form/orientation/scale/homogeneity/density of nanoarrays are investigated through a series of Raman measurements in order to better understand this nano-templated approach.

[a] *Centre de Nanosciences et de Nanotechnologies, CNRS, Univ Paris Sud, Université Paris Saclay, C2N-Orsay, 91405 Orsay, France. E-mail: gregory.barbillon@laposte.net*
[b] *Nanovation SARL, 8 Route de Chevreuse, 78117 Chateaufort, France.*
[c] *Laboratoire de Chimie Physique, CNRS, Univ Paris Sud, Université Paris Saclay, Bâtiment 201 Porte 2, 91405 Orsay, France.*
[d] *Center for Quantum Devices, Department of Electrical and Computer Engineering, Northwestern University, Evanston, Illinois 60208, USA.*

2 Experimental section

2.1 Fabrication of Au/ZnO nanostructures

Self organising arrays of ZnO nanostructures were grown on silicon (111) and c-plane sapphire (c-Al_2O_3) substrates by pulsed laser deposition (PLD) from a 99.99% pure ZnO target using a KrF excimer laser (248 nm), as described elsewhere[31–33]. A ZnO thin film buffer layer was grown on the substrates in order to seed the nanostructure growth. Substrate temperature was between 600 °C and 700 °C for all nanostructure growths. In this paper, the samples fabricated on silicon and on c-sapphire are called Si and Sa, respectively (see Table 1). A gold layer of 30 *nm* was deposited on all samples by either thermal evaporation (TE)[31], or electron beam evaporation (EBE). The sample morphology was studied using a Philips XL-30 SEMFEG.

2.2 Thiophenol functionalization on Au/ZnO nanostructures

In order to study the use of the Au/ZnO nanostructures for SERS sensing, thiophenol was adopted as a probe molecule (selected based on the known suitability for grafting onto a gold surface). The functionalization protocol was as follows: (i) preparation of a 1 *mM* solution of thiophenol in ethanol, (ii) immersion of the sample in the solution for 24 h, (iii) rinsing thoroughly with pure ethanol, (iv) drying with molecular nitrogen. For the Raman measurements in solution (non-SERS reference measurements: thiophenol in ethanol) a thiophenol concentration of 1 M was used.

2.3 Optical characterization by Raman spectroscopy

A Labram spectrophotometer from Horiba Scientific with a spectral resolution of 1 cm^{-1} was employed for the Raman studies. A He-Ne laser with an excitation wavelength λ_{exc} of 633 *nm* and a power of $\sim$ 1 *mW* was used for all measurements. The laser was focused on the substrate with a microscope objective ($\times$ 100, N.A. = 0.9). The SERS signal from the Au/ZnO nanostructures was collected using the same objective in a backscattering configuration. The same excitation wavelength and a macro-objective with a focal length of 40 *mm* (N.A. = 0.18) were used for standard (i.e. non-SERS reference) Raman measurements in solution. The acquisition time was fixed at 20 *s* and all the spectra presented here correspond to raw data without any background subtraction and were normalized for acquisition time and laser power for comparison purposes. The average SERS intensities and Relative standard deviations (RSD) were calculated based on 20 SERS spectra. The I_{SERS}/I_{Raman} ratios were calculated based on average values of SERS intensity.

3 Results and discussion

Representative SEM images of the various Au/ZnO nanostructure arrays are displayed in Figure 1. For all the samples, the nanoarrays show a regular nanopillar form and a preferential vertical orientation. It should be noted that some within-wafer variation of nanostructure scale, filling factor, form and orientation was observed, however. This was most likely due to the inhomogeneous plasma plume used for the PLD deposition. Although the nanopillars appear to be rounded at the tips, it was found in previous studies that they are actually hexagonally faceted and the rounded form is an illusion resulting from the transparency induced by the elevated electron accelerating voltage in the SEM[34]. All the nanopillars grown on silicon substrates showed relatively tight width distributions (from $\sim$ 240 *nm* for Si1 to $\sim$ 340 *nm* for Si4) while the filling factors varied more significantly (from a very dense and oriented structure in Si3 to a much more open and disoriented structure in Si1). For the Si1 and Si2 samples the nanopillar width is smaller than for samples Si3 and Si4, and the nanostructures are not as preferentially aligned along the growth direction. In previous studies, it was shown that the nanostructure pitch and orientation are dictated, respectively, by the grain size[34] and crystallographic orientation[35] in the underlying ZnO buffer layer which is used to seed vertically oriented arrays. Both the smaller grain sizes and the increased dispersions in nanopillar orientation for samples Si1/Si2 compared to samples Si3/Si4 may be due, therefore, to the buffer layer being thinner (as a result of plasma plume variations). The logic is that there is a critical buffer layer thickness required for the predominance of grains with the wurtzite *c*-axis aligned along the growth direction to emerge. The nanostructures grown on the sapphire substrates also all show dense arrays with strong preferential orientation along the growth direction but exhibit less regular form and a broader range of nanopillar widths ranging from $\sim$ 180 *nm* (for sample Sa4) up to $\sim$ 900 *nm* (for sample Sa3). This less regular form of nanostructures for growths on sapphire compared to silicon was observed in previous studies[31] and attributed to an in-plane widening of the buffer-layer grains due to an epitaxial relationship with the sapphire.

Figure 2 reveals the SERS spectra for Au/ZnO nanostructures (after grafting of the thiophenol molecules) obtained with an excitation wavelength of 633 nm. For all 8 sample types, strong Raman peaks characteristic of thiophenol molecules[36,37] were observed at 1000 cm^{-1}, 1025 cm^{-1} and 1075 cm^{-1}. They correspond, respectively, to an out-of-plane C-C-C stretching vibration mode, an out-of-plane C-H stretching vibration mode, and an in-plane C-C-C stretching vibration mode along with a C-S stretching vibration mode. In the following the SERS responses of 9 pairs of samples with all but one growth parameter fixed are compared in light of the various nanostructure morphologies in order to gain insight on the factors impacting the average SERS intensity and the reproducibility.

3.1 Paired Comparisons for Samples with Parameters Other than Substrate Held Constant

Two paired comparisons were considered in which all other variables than the underlying substrate were held constant: (a) 600 °C ZnO growth with EBE gold coating (samples Si1 and Sa1) and (b) 700 °C ZnO growth with TE gold coating (samples Si4 and Sa4). For paired comparison (a), average SERS intensity was higher for the Sa substrate than for the Si substrate for all three 3 Raman peaks studied here (see Figure 3). For sample Si1, the nanopillars were of similar width but not as preferentially aligned as those for samples Sa1. Hence, the nanopillar density and filling

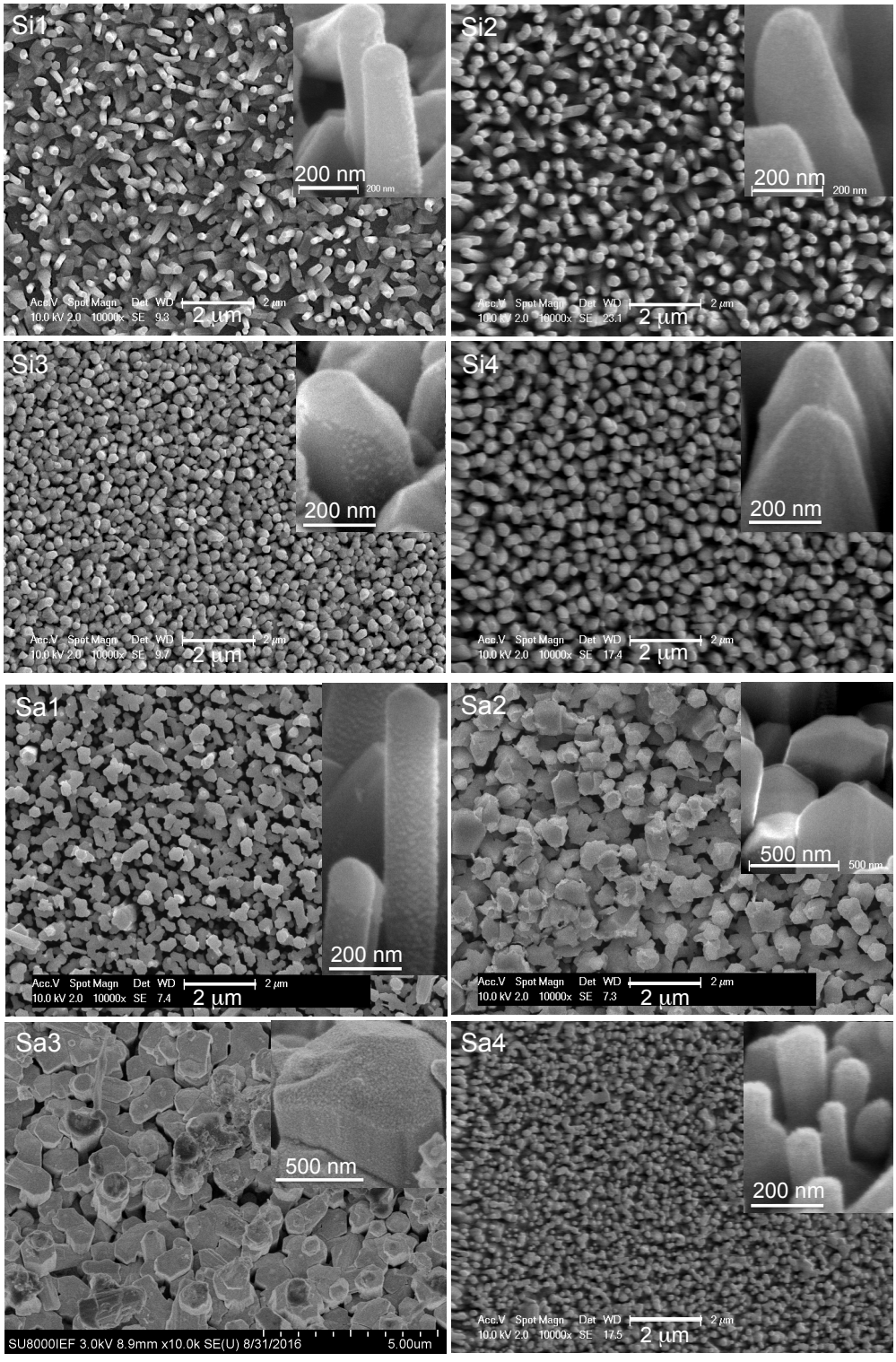

Fig. 1 SEM images for the Au/ZnO nanostructures grown on silicon (Si1, Si2, Si3, Si4) and sapphire substrates (Sa1, Sa2, Sa3, Sa4).

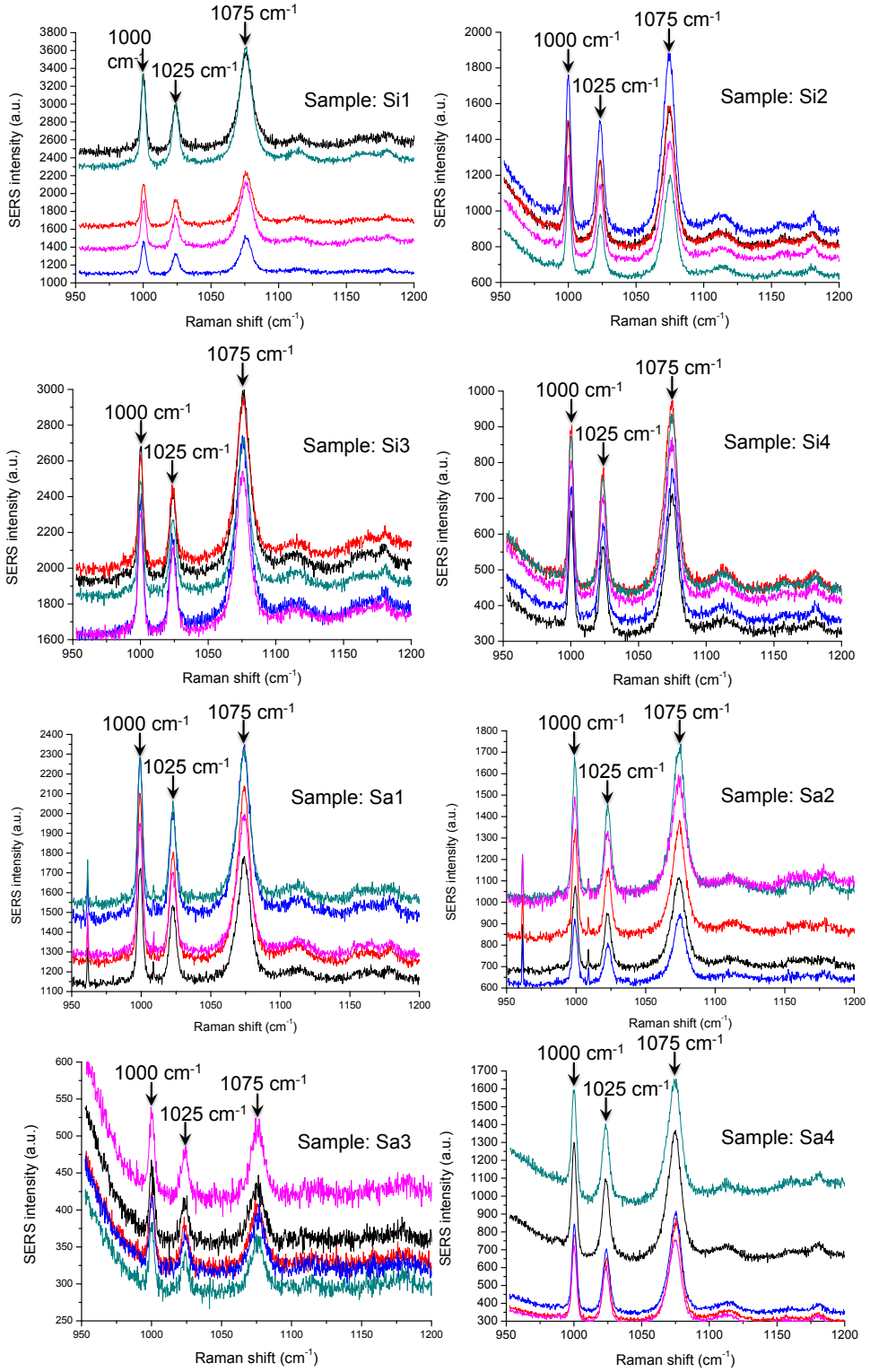

Fig. 2 SERS spectra (acquired at different positions on 1 cm^2 substrates) for thiophenol molecules grafted on Au/ZnO nanostructure arrays on silicon substrates: Si1, Si2, Si3, Si4, and sapphire substrates: Sa1, Sa2, Sa3 and Sa4.

Name	Substrate	T (°C)	Dep. met.	density (NP/μm^2)	W (nm)	f
Si1	Silicon	600	EBE	4.12	240	0.19
Si2	Silicon	600	TE	4.92	260	0.26
Si3	Silicon	700	EBE	10.08	310	0.77
Si4	Silicon	700	TE	7.89	340	0.73
Sa1	Sapphire	600	EBE	10.32	280	0.63
Sa2	Sapphire	650	EBE	2.98	590	0.81
Sa3	Sapphire	650	TE	1.38	900	0.88
Sa4	Sapphire	700	TE	23.75	180	0.61

Table 1 Sample names with their parameters of fabrication: substrate, ZnO nanostructure growth temperature (T), Au deposition method (Dep. met.), and the nanopillar (NP) density, average width W and filling factor f.

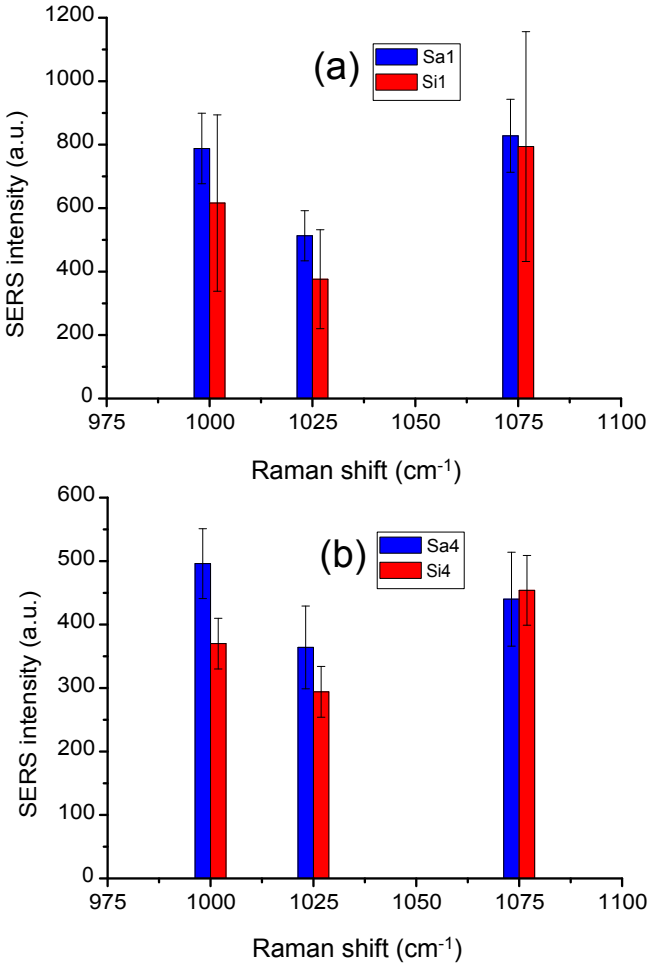

Fig. 3 Values of SERS intensity and RSD (Intensity ± RSD) for the three characteristic thiophenol Raman peaks at 1000 cm^{-1}, 1025 cm^{-1} and 1075 cm^{-1}, for the two paired comparisons (a) and (b) described in section 3.1.

factor were lower. Moreover, a significantly better within-wafer reproducibility of the SERS signal was obtained for sample Sa1 (see Figure 3). This may be related to the more regular arrangement of nanopillars (Sa1). For the Sa4/Si4 paired comparison (b), the average SERS intensity was also higher for the Sa substrate than for the Si substrate while a slightly better within-wafer homogeneity of SERS signal was obtained for the growth on the Si substrate (see Figure 3). In this case, the SEM images and table 1 reveal that the main obvious differences in morphology are the smaller width along with a higher density for the nanopillars grown on sapphire. In summary, two paired comparisons (with ZnO nanostructure growth temperature and gold deposition method held constant) were consistent with finer and more oriented nanopillars giving a higher SERS response and better within-wafer reproducibility.

3.2 Paired Comparisons for Samples with Parameters Other than ZnO Nanostructure Growth Temperature Held Constant

Four paired comparisons were considered in which direct variables other than ZnO nanostructure growth temperature were held constant (see Figure 4). In case (a) the substrate was Si and the Au coating was deposited using EBE (Si1 and Si3). The second case (b) involved Si substrates and TE coating with gold (Si2 and Si4). The third case (c) concerned sapphire substrates and EBE coating with gold (Sa1 and Sa2). The last case (d) considered sapphire substrates and TE coating with gold (Sa3 and Sa4).

For the Si1/Si3 paired comparison (a), the higher ZnO nanostructure growth temperature correlated with a slightly higher average SERS intensity and a much better within-wafer signal reproducibility (see Figure 4). Based on the SEM images and table 1, the increase in SERS intensity correlates with a higher density, stronger alignment and a higher filling factor. The improved within-wafer reproducibility for Si3 may again be a result of the more regular arrangement of the aligned nanopillars, as discussed in 3.1(a) above. Paired comparison (b) shows a higher average SERS intensity for the less oriented nanopillars with a smaller width grown at lower temperature. The within-wafer reproducibility is better for the higher temperature ZnO deposition which again correlates with more regular and aligned arrays with a higher filling factor, as in 3.1(a) and 3.2(a). In paired

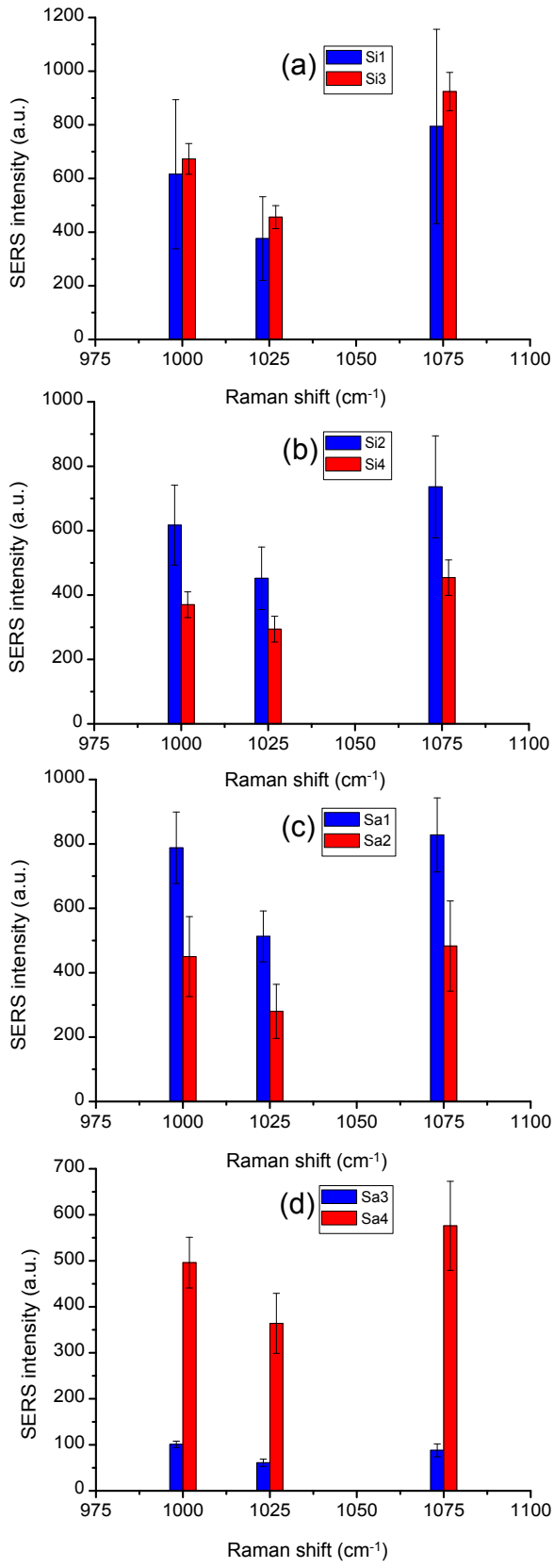

Fig. 4 Values of SERS intensity and RSD (Intensity $\pm$ RSD) for the three characteristic thiophenol Raman peaks at 1000 cm^{-1}, 1025 cm^{-1} and 1075 cm^{-1}, for the four paired comparison cases (a), (b), (c) and (d) described in section 3.2.

comparison (c) the samples showed similar reproducibility and the lower growth temperature sample (Sa1) gave higher average SERS intensities. SEM images (figure 1) show that although there is a similar strong vertical orientation for both samples, there are much smaller widths for the nanostructures grown at lower temperature, a higher density (see Table 1) and a better homogeneity of form. For the last paired comparison (d) much higher values of average SERS intensity are observed for the more elevated ZnO nanostructure growth temperature. For this sample (Sa4), the average nanopillar width is much smaller than for the lower temperature sample (Sa3), and the density is higher (see Table 1). However, a better reproducibility is obtained for the lowest temperature of ZnO nanostructure growth. In summary, the paired comparisons for different growth temperatures do not show a clear correlation between growth temperature and average SERS intensity but they are coherent with the findings in section 3.1 that narrower nanopillars give stronger SERS signals while more aligned nanopillars give better reproducibility. They are also coherent with the potential correlation of increased SERS intensity with nanopillar orientation that was evoked in section 3.1.

3.3 Paired Comparison for Samples with Parameters Other Than Gold Deposition Method Held Constant

Three paired comparisons were considered in which direct variables other than the gold deposition method were held constant (see Table 1). In the first paired comparison (a) the substrate was Si and the growth temperature was 600°C (Samples: Si1 and Si2). The second case (b) also considered Si substrates but with a growth temperature of 700°C (Samples: Si3 and Si4). The final paired comparison (c) investigated Sa substrates for a fixed growth temperature of 650°C (Samples: Sa2 and Sa3).

For paired comparison (a) (see Figure 5) the average SERS intensity was relatively similar for the layer coated with the two techniques. However, a significantly better reproducibility of SERS signal was obtained for the TE technique (sample Si2). While the density, width and filling factor are similar for the two samples the SEM images in Figure 1 show that sample Si2 has more preferential vertical orientation of nanostructures. For case (b) the SERS intensity is significantly higher for the Si3 sample with EBE gold deposition. This could be due to the smaller nanopillar width, the higher density and the slightly higher filling factor for sample Si3. The reproducibility is similar for samples Si3 and Si4. For paired comparison (c), higher values of SERS intensity are obtained for sample Sa2 than sample Sa3 and this again correlates with a higher density and a smaller width. However, a much better reproducibility is obtained with the TE method for sample Sa3. This may be related to the slightly higher filling factor. In summary, paired comparisons based on fixing all parameters except the gold deposition method are coherent with the hypotheses developed in sections 3.1 and 3.2 that smaller nanopillar widths correlate with stronger SERS signal while denser and more aligned arrays give better within-wafer reproducibility.

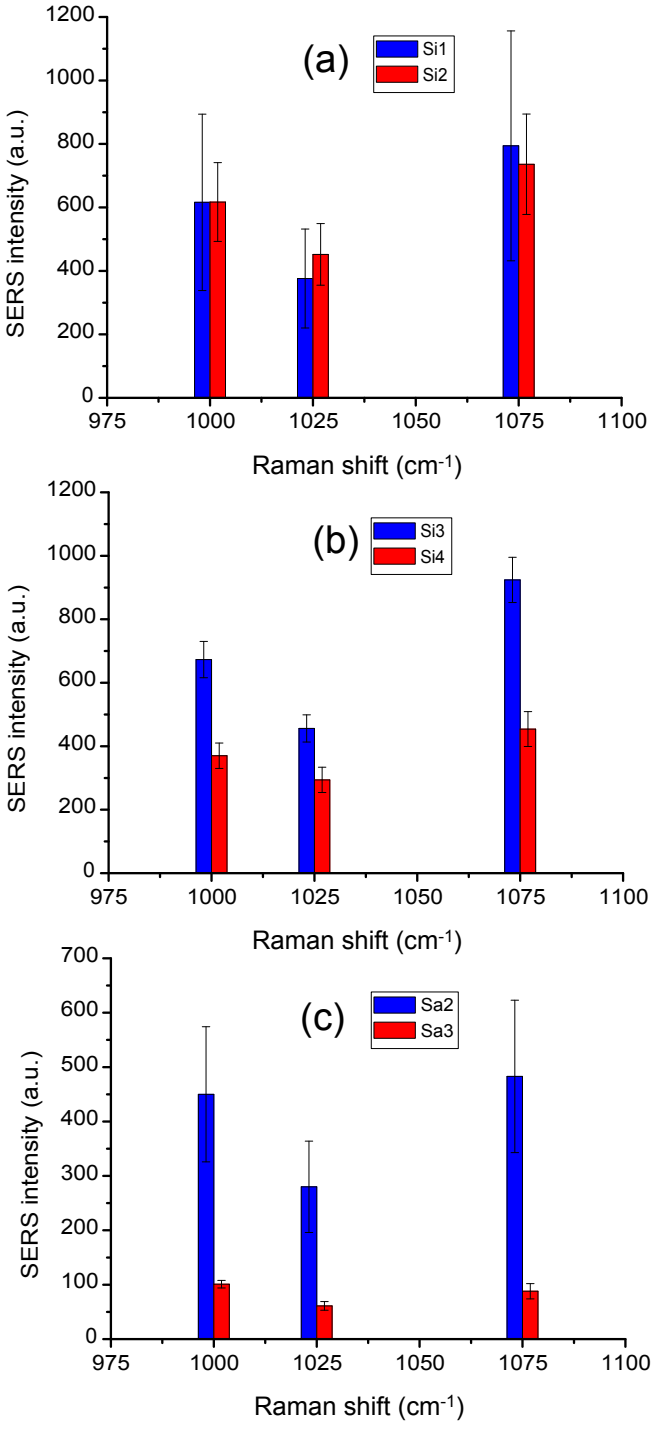

Fig. 5 Values of SERS intensity and RSD (Intensity ± RSD) for the three characteristic thiophenol Raman peaks at 1000 cm^{-1}, 1025 cm^{-1} and 1075 cm^{-1}, for three paired comparisons (a), (b), and (c) described in section 3.3.

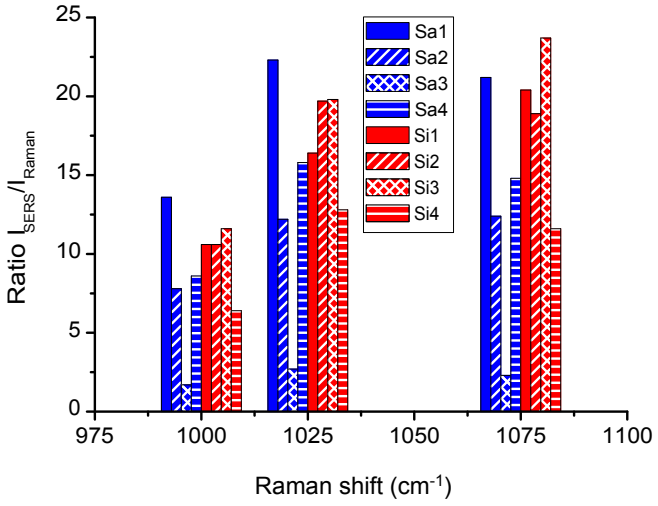

Fig. 6 Ratio I_{SERS}/I_{Raman} for the three characteristic Raman peaks at 1000 cm^{-1}, 1025 cm^{-1} and 1075 cm^{-1} for all the studied samples at an excitation wavelength of 633 nm.

3.4 Calculation of the ratio I_{SERS}/I_{Raman}

In order to evaluate the SERS sensitivity, the enhancement factor (EF) is usually calculated. EF is given by the general equation:

$$EF = \frac{I_{SERS}}{I_{Raman}} \times \frac{N_{Raman}}{N_{SERS}} \quad (1)$$

where I_{SERS}, I_{Raman} represent the SERS and Raman intensities, respectively. N_{SERS}, N_{Raman} are the number of excited molecules in SERS and Raman experiments (thiophenol in ethanol), respectively. However, as demonstrated by Le Ru *et al.*[38], this general formula is limited by major constraints when there is a complex morphology such as in our nanostructures. Indeed, N_{SERS} is difficult to evaluate in our case. Hence, the ratio I_{SERS}/I_{Raman} was taken as an estimate of the sensitivity for our Au/ZnO nanostructures. The values of I_{Raman} are equal to 58, 23, 39 for the Raman peaks at 1000 cm^{-1},1025 cm^{-1} and 1075 cm^{-1}, respectively. These values are extracted from the Raman spectrum available in reference[21].

From Figure 6, it was observed that the samples Sa1 and Si3 had the highest values of I_{SERS}/I_{Raman} for the 1000 cm^{-1}, 1025 cm^{-1} and 1075 cm^{-1} Raman peaks. The figure shows no clear correlation between substrate type and I_{SERS}/I_{Raman}. Although it may be incidental, it can also be seen from Figure 6 (with reference to Table 1) that the values of I_{SERS}/I_{Raman} are generally higher when the Au deposition was done by EBE.

4 Conclusion

In this paper, eight 1 cm^2 samples of self-organising ZnO nanopillar arrays with preferential vertical orientation were grown by pulsed laser deposition and then coated with 30 nm of Au using either thermal or electron-beam evaporation. Each sample had a different set of ZnO and Au growth conditions. The Au/ZnO nanoarrays were then tested for use in SERS detection of thiophenol molecules. The ratio of I_{SERS}/I_{Raman} was adopted as a measure of the SERS sensitivity and was found to vary from 1.7

to 23.7 within the 8 samples. The impact of the width, filling factor, orientation, homogeneity and shape of the nanostructures on the average SERS intensity and the within-wafer reproducibility of the SERS response were considered for 9 paired comparisons based on fixing all but one of the growth parameters for each pairing. Overall, smaller nanopillar width with a high density was found to correlate with stronger average SERS signal while more vertically aligned arrays with higher filling factors showed better within-wafer reproducibility. Based on these findings, optimisation can now be conducted in order to produce Au/ZnO nanostructures which could serve as relatively inexpensive and high performance self-forming SERS sensing platforms with improved reproducibility compared to existing technologies.

References

1 D. Jimenez de Aberasturi, A. B. Serano-Montes, J. Langer, M. Henriksen-Lacey, W. J. Parak and L. M. Liz-Marzan, *Chem. Mater.*, 2016, **28**, 6779.

2 A. La Porta, A. Sanchez-Iglesias, T. Altantzis, S. Bals, M. Grzelczak and L. M. Liz-Marzan, *Nanoscale*, 2015, **7**, 10377.

3 L. Dalstein, M. Ben Haddada, G. Barbillon, C. Humbert, A. Tadjeddine, S. Boujday and B. Busson, *J. Phys. Chem. C*, 2015, **119**, 171476.

4 Q. Wang, G. Lu, L. Hou, T. Zhang, C. Luo, H. Yang, G. Barbillon, F. H. Lei, C. A. Marquette, P. Perriat, O. Tillement, S. Roux, Q. Ouyang and Q. Qong, *Chem. Phys. Lett.*, 2011, **7**, 256.

5 R. Gillibert, M. Sarkar, J. F. Bryche, R. Yasukuni, J. Moreau, M. Besbes, G. Barbillon, B. Bartenlian, M. Canva and M. Lamy de la Chapelle,*Nanotechnology*, 2016, **27**, 115202.

6 M. Sarkar, M. Besbes, J. Moreau, J. F. Bryche, A. Olivéro, G. Barbillon, A. L. Coutrot, B. Bartenlian and M. Canva, *ACS Photonics*, 2015, **2**, 237.

7 Q. Yu, P. Guan, D. Qin, G. Golden and P. M. Wallace, *Nano Lett.*, 2008, **8**, 1923.

8 G. Barbillon, J. L. Bijeon, G. Lérondel, J. Plain and P. Royer, *Surf. Sci.*, 2008, **602**, L119.

9 H. J. Ahn, P. Thiyagarajan, L. Jia, S. I. Kim, J. C. Yoon, E. L. Thomas and J. H. Jang, *Nanoscale*, 2013, **5**, 1836.

10 T. Vo-Dinh, A. Dhawan, S. J. Norton, C. G. Khoury, H. N. Wang, V. Misra and M. D. Gerhold, *J. Phys. Chem. C*, 2010, **114**, 7480.

11 A. Dhawan, A. Duval, M. Nakkach, G. Barbillon, J. Moreau, M. Canva and T. Vo-Dinh, *Nanotechnology*, 2011, **22**, 165301.

12 A. C. Faure, G. Barbillon, M. Ou, G. Ledoux, O. Tillement, S. Roux, D. Fabregue, A. Descamps, J. L. Bijeon, C. A. Marquette, C. Billotey, C. Jamois, T. Benyatou and P. Perriat, *Nanotechnology*, 2008, **19**, 485103.

13 J. F. Bryche, R. Gillibert, G. Barbillon, M. Sarkar, A. L. Coutrot, F. Hamouda, A. Aassime, J. Moreau, M. Lamy de la Chapelle, B. Bartenlian and M. Canva, *J. Mater. Sci.*, 2015, **50**, 6601.

14 J. F. Bryche, R. Gillibert, G. Barbillon, P. Gogol, J. Moreau, M. Lamy de la Chapelle, B. Bartenlian and M. Canva, *Plasmonics*, 2016, **11**, 601.

15 G. Barbillon, F. Hamouda, S. Held, P. Gogol and B. Bartenlian, *Microelectron. Eng.*, 2010, **87**, 1001.

16 G. Barbillon, *Micromachines*, 2012, **3**, 21.

17 M. Cottat, N. Lidgi-Guigui, I. Tijunelyte, G. Barbillon, F. Hamouda, P. Gogol, A. Aassime, J. M. Lourtioz, B. Bartenlian and M. Lamy de la Chapelle, *Nanoscale Res. Lett.*, 2014, **9**, 623.

18 J. F. Bryche, A. Tsigara, B. Bélier, M. Lamy de la Chapelle, M. Canva, B. Bartenlian and G. Barbillon, *Sens. Actuator B-Chem*, 2016, **228**, 31.

19 J. F. Masson, K. F. Gibson and A. Provencher-Girard, *J. Phys. Chem. C*, 2010, **114**, 22406.

20 J. P. Camden, J. A. Dieringer, J. Zhao and R. P. Van Duyne, *Accounts Chem. Res.*, 2008, **41**, 1653.

21 J. F. Bryche, B. Bélier, B. Bartenlian and G. Barbillon, *Sens. Actuator B-Chem*, 2017, **239**, 795.

22 H. Wang, X. Jiang, S. T. Lee and Y. He, *Small*, 2014, **10**, 4455.

23 M. L. Zhang, X. Fan, H. W. Zhou, M. W. Shao, J. Antonio Zapien, N. B. Wong and S. T. Lee, *J. Phys. Chem. C*, 2010, **114**, 1969.

24 M. S. Schmidt, J. H*ü*bner and A. Boisen, *Adv. Mater.*, 2012, **24**, OP11.

25 E. Galopin, J. Barbillat, Y. Coffinier, S. Szunerits, G. Patriarche and R. Boukherroub, *ACS Appl. Mater. Interfaces*, 2010, **1**, 1396.

26 S. Cui, Z. Dai, Q. Tian, J. Liu, X. Xiao, C. Jiang, W. Wu and V. A. L. Roy, *J. Mater. Chem. C*, 2016, **4**, 6371.

27 L. Liu, H. Yang, X. Ren, J. Tang, Y. Li, X. Zhang and Z. Cheng, *Nanoscale*, 2015, **7**, 5147.

28 G. Sinha, L. E. Depero and I. Alessandri, *ACS Appl. Mater. Interfaces*, 2011, **3**, 2557.

29 C. Cheng, B. Yan, S. M. Wong, X. Li, W. Zhou, T. Yu, Z. Shen, H. Yu and H. J. Fan, *ACS Appl. Mater. Interfaces*, 2010, **2**, 1824.

30 M. A. Khan, T. P. Hogan and B. Shanker, *J. Raman Spectrosc.*, 2009, **40**, 1539.

31 V. E. Sandana, D. J. Rogers, F. Hosseini Teherani, R. McClintock, C. Bayram, M. Razeghi, H. J. Drouhin, M. C. Clochard, V. Sallet, G. Garry and F. Falyouni, *J. Vac. Sci. Technol. B*, 2009, **27**, 1678.

32 D. J. Rogers, D. C. Look, F. Hosseini Teherani, K. Minder, M. Razeghi, A. Largeteau, G. Demazeau, J. Morrod, K. A. Prior, A. Lusson and S. Hassani, *phys. stat. sol. (c)*, 2008, **5**, 3084.

33 D. J. Rogers, V. E. Sandana, F. Hosseini Teherani, M. Razeghi and H. J. Drouhin, *Proc. SPIE*, 2009, **7217**, 721708-1.

34 V. E. Sandana, D. J. Rogers, F. Hosseini Teherani, P. Bove and M. Razeghi, *phys. stat. sol. (a)*, 2014, **211**, 449.

35 R. Erdelyi, T. Nagata, D. J. Rogers, F. Hosseini Teherani, Z. E. Horvath, Z. Labadi, Z. Baji, Y. Wakayama and J. Volk, *Cryst. Growth Des.*, 2011, **11**, 2515.

36 C. Humbert, O. Pluchery, E. Lacaze, A. Tadjeddine and B. Busson, *Phys. Chem. Chem. Phys.*, 2012, **14**, 280.

37 K. T. Carron and L. Gayle Hurley, *J. Phys. Chem.*, 1991, **95**, 9979.

38 E. C. Le Ru, E. Blackie, M. Meyer and P. G. Etchegoin, *J. Phys. Chem. C*, 2007, **111**, 13794.